

Elastic Softening in Synthetic Diamonds

Tatsuya Yanagisawa,¹ Ruo Hibino,¹ Hiroyuki Hidaka,¹ Hiroshi Amitsuka,¹ Toshiyuki Tashima,² Mitsuhiro Akatsu,³ Yuichi Nemoto,³ Sergei Zherlitsyn,⁴ and Joachim Wosnitza^{4,5}

¹*Department of Physics, Hokkaido University, Sapporo 060-0810, Japan*

²*Department of Electronic Science and Engineering, Kyoto University, Kyoto 615-8510, Japan*

³*Graduate School of Science and Technology, Niigata University, Niigata 950-2181, Japan*

⁴*Hochfeld-Magnetlabor Dresden (HLD-EMFL) and Würzburg-Dresden Cluster of Excellence ct.qmat, Helmholtz-Zentrum Dresden-Rossendorf (HZDR), 01328 Dresden, Germany*

⁵*Institut für Festkörper- und Materialphysik, TU Dresden, 01062 Dresden, Germany*

(Dated: May 9, 2025)

This study reveals a previously unreported phenomenon: elastic softening of synthetic diamonds at temperatures below 1 K. We present ultrasonic measurements on single-crystalline, non-irradiated synthetic diamonds—namely, type-IIa (colorless) and type-Ib (yellow) diamonds grown by high-pressure high-temperature (HPHT) synthesis, as well as type-IIa diamond grown by chemical vapor deposition (CVD). A pronounced, divergent decrease in the elastic stiffness constant C_{44} was observed in all samples down to 20 mK. We attribute this softening to electric quadrupolar degrees of freedom with irreducible representation T_2 in diamond. The microscopic origin of this effect, however, remains unresolved. By analogy with similar behavior observed in silicon, we suggest the presence of an as-yet-unidentified, defect-derived quantum ground state with T_1 or T_2 symmetry at ppb-level concentrations in all three diamonds studied.

Diamonds have long attracted interest not only for their aesthetic value but also for their exceptional physical properties. Since ancient times, impurities and defects in diamonds have played a critical role in their appraisal as gemstones. Diamonds exhibit different colors depending on the type and concentration of impurities within the crystal. A yellow hue typically indicates dominant nitrogen impurities (type Ib), whereas a blue color is associated with boron as the primary impurity (type IIb). Two types of colorless diamonds exist: type Ia, which contains nitrogen in dimer form, and type IIa, which contains only trace impurities.

In recent years, the development of synthetic diamond growth techniques has attracted attention not only for semiconductor applications [1], but also for exploring quantum properties of defects and their potential technological uses [2–5]. In particular, spin states associated with atomic vacancies in diamond are regarded as promising candidates for solid-state quantum sensors, with applications ranging from life sciences to materials research [6–9]. These spin states also offer a platform for fundamental studies in quantum physics and pave the way toward quantum technologies, including quantum computation and communication [10–15]. Most diamond-based quantum technologies to date have relied on commercially available synthetic diamonds fabricated via high-pressure high-temperature (HPHT) or chemical vapor deposition (CVD) methods.

More recently, significant advances in diamond synthesis technologies have enabled the growth of large, high-quality single crystals. The HPHT flux and CVD methods are now commonly employed to produce type-IIa diamonds with extremely low vacancy concentrations. However, the formation of single-atom vacancies at the sub-

ppb level is thermodynamically unavoidable during the growth process [16] and must be carefully controlled for quantum technology applications. Previous studies have primarily reported ppm-level concentrations of neutral single vacancies (V_0) [Fig. 1(a)], inferred from zero-phonon lines of optical centers attributed to V_0 [17–19].

Although numerous studies have explored the engineering of nitrogen-vacancy (NV) color centers [Fig. 1(c) middle] defect states formed by radiation-induced atomic vacancies adjacent to nitrogen atoms [20–23] only limited attention has been given to the intrinsic structure and quantum properties of defect centers in non-irradiated diamonds, owing to the extremely low concentration of vacancies. In particular, the quantum ground state of single atomic vacancies in non-irradiated synthetic diamonds, which are widely used as substrates for quantum devices, remains largely unexplored. Here, the term quantum ground state encompasses not only the spin state, but also the many-body ground state arising from electron-phonon coupling at the vacancy site. Understanding these intrinsic quantum states at cryogenic temperatures is essential for the rational development of next-generation quantum technologies.

Here, we report a pronounced softening of the transverse elastic stiffness constant, C_{44} , revealed by ultrasonic measurements below 1 K. This elastic softening may arise from electric quadrupolar degrees of freedom, indicating the presence of an as-yet-unidentified, defect-derived non-magnetic quantum ground state with T_1 or T_2 symmetry at ppb-level concentrations.

Diamond has a cubic crystal structure (O_h^7 , $Fd\bar{3}m$, No. 227) with lattice constant $a = 3.567\text{Å}$ [24], as schematically shown in Fig. 1(a). The sp^3 orbitals of carbon with the outermost electron configuration $(2s)^2(2p)^2$ are

covalently bound to each other, and thereby, form the diamond structure, resulting in one of the hardest materials on earth. We used three non-irradiated commercially available synthetic diamond species grown by HPHT synthesis (Sample 1 and 3) and CVD (Sample 2) for our ultrasonic measurements presented here.

Sample 1 is a 0.16 carat mono-sectorial type-IIa (colorless) HPHT diamond (New Diamond Technology), with a length of 3.043 mm along the [110] direction and a thickness of ~ 1.0 mm along the [001] direction. According to the manufacturer, the B and N concentrations in this type-IIa HPHT diamond without irradiation process are expected to be ~ 50 ppb and ~ 10 ppb, respectively. Sample 2 is a type-IIa CVD-grown diamond single crystal, so called ‘Electronic Grade’ (Element Six) without irradiation, which has a B concentration of less than 1 ppb and a N concentration of 0.1-1 ppb, and natural abundance of ^{13}C impurity ($98.892 : 1.108 = ^{12}\text{C} : ^{13}\text{C}$). The dimension of the sample is $2.060 \times 2.18 \times 0.504 \text{ mm}^3$. Sample 3 is a non-irradiated type-Ib (yellow) HPHT diamond (Sumitomo Electric), trade name SUMICRYSTAL (UP $3 \times 3 \times 2$ 100c), with a length of 2.944 mm along the [001] direction and a thickness of ~ 2.0 mm along the [100] direction.

Ultrasound was generated and detected by using a pair of LiNbO_3 resonance transducers of $100 \mu\text{m}$ thickness (with fundamental frequency of ~ 18 MHz), which are bonded on the polished sample surfaces with room-temperature-vulcanizing silicone. We measured the elastic constant C_{44} of sample 1 using the transverse ultrasonic wave propagating along [110] with polarization along the [001] axis, which induced the elastic strain $\frac{1}{\sqrt{2}}(\varepsilon_{yz} + \varepsilon_{zx})$. Similarly, we measured C_{44} in samples 2 and 3 using the transverse wave propagating along [001] with polarization along the [100] axis, which induced the elastic strain ε_{zx} . We converted the sound velocity v_{ij} to the elastic constant C_{ij} using the formula $C_{ij} = \rho v_{ij}^2$, [25] where $\rho = 3.515 \text{ g/cm}^3$ is the calculated density of diamond. We calculated the absolute value using the measured sound velocity of 12733 m/s at 1 K.

For our low-temperature ultrasonic measurements, we used two different ^3He - ^4He dilution refrigerators: top-loading, wet- type for Samples 1 (0.025-0.65 K) and 3 (0.025-0.65 K), and dry-type for Sample 2 (0.025-2.0 K), and ^3He refrigerators for Samples 1 (0.5-2.0 K). Measurements above 2 K were made using PPMS (Quantum Design Inc.). Magnetic fields up to 16.5 T were generated by superconducting magnets.

The temperature dependence of the elastic constant C_{44} at zero magnetic field is shown in Figs. 2(a) and 2(c) for single-crystalline HPHT type-IIa diamond (Sample 1). C_{44} gradually hardens down to ~ 1 K [as shown in Fig. 2(c)], which is a general behavior of solids owing to the anharmonicity of acoustic phonons. This change is consistent with previously reported temperature de-

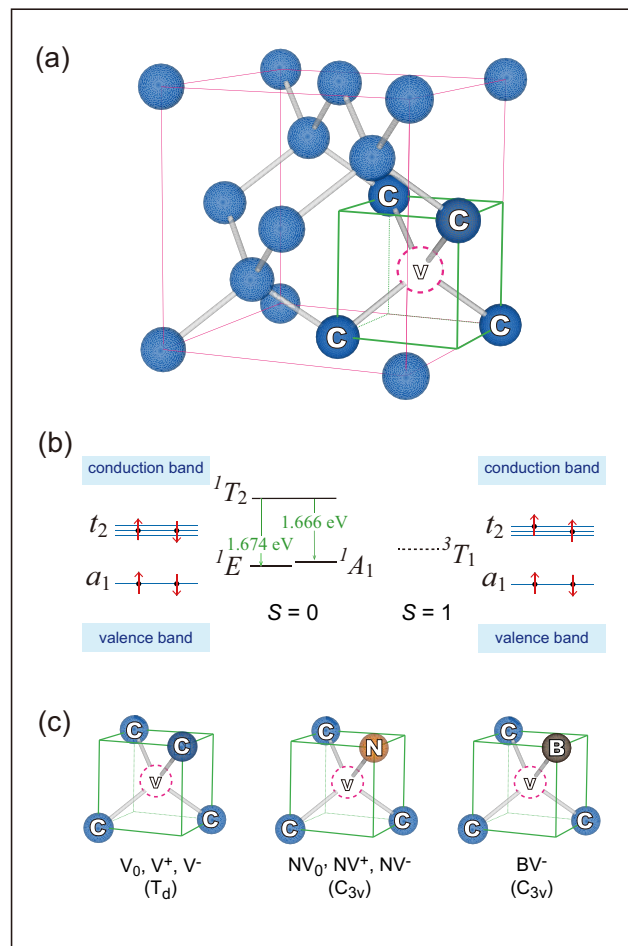


FIG. 1. (a) Diamond crystal structure with a single atomic vacancy in a unit cell. (b) Electron occupation of the ground-state molecular orbitals configuration [26], and energy level structure of V_0 [27]. The red arrows represent electron spins and their arrangement. The optically inactive 3T_1 state of V_0 is indicated by dashed line. (c) Schematic illustrations of common defects with atomic vacancies in non-irradiated diamond; (from left) single atomic vacancies, NV centers (a nitrogen atom adjacent to a vacancy), BV^- center (a boron atom adjacent to a vacancy). The symmetry of each defect is also represented.

pendences of the sound velocity of transverse ultrasonic waves measured down to ~ 10 K [28–30]. To the best of our knowledge, no previous work has yet studied the elastic constants of diamond below 1 K. The low-temperature region of C_{44} exhibits 125 ppm softening from 1 K down to 20 mK. These results indicate that the sites causing elastic softening locally preserve the tetrahedral T_d symmetry even at 20 mK. Figure 2(b) shows the magnetic-field dependence of C_{44} at 25 mK and 2 K with shifted offset for the 2 K data. The magnetic field is applied along the [001] direction. The 125 ppm softening is almost unchanged for magnetic fields up to 16.5 T.

Further, we investigated the elastic response for other

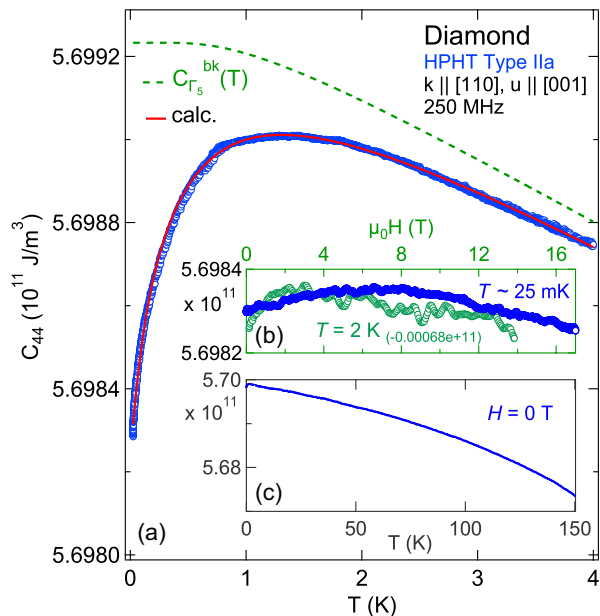


FIG. 2. (a) Temperature dependence of the elastic constant C_{44} for single-crystalline synthetic HPHT diamond (type IIa) below 4 K at zero magnetic field compared to calculations (solid red curve) based on the orbital analogue of the Curie-Weiss law (see text). The green dashed line represents the background term $C_{\Gamma_5}^{bk}$ owing to phonons uncoupled to the electronic system. (b) Magnetic-field dependence of C_{44} at 25 mK (blue) and 2 K (green) with shifted offset for the 2 K data. The magnetic field is applied along the [001] direction. (c) Temperature dependence of the elastic constant C_{44} for a wide temperature region up to 150 K.

diamonds grown by different methods. Figure 3 shows the temperature dependence of C_{44} for three different types of diamonds. The inset of Fig. 3 shows data up to 100 K on a logarithmic temperature axis. Sample 1 is the type-IIa HPHT diamond with data already shown in Fig. 2. Sample 2 is also a type-IIa diamond grown by CVD. Sample 3 is a HPHT yellow diamond of type Ib that presumably contains numerous nitrogen impurities. Sample 1 and 2 show a nearly identical low-temperature softening within the resolution of the present measurements. The data for Sample 2 are noisy because of the small sample thickness. The softening in Sample 3 (type-Ib HPHT) is only approximately 1/3 of that of the Samples 1 (type-IIa HPHT) and 2 (type-IIa CVD). Obviously, the defect concentration responsible for the softening in sample 3 is lower than in samples 1 and 2. Notably, the low-temperature softening shows nearly zero magnetic-field dependence up to 14.0 - 16.5 T (Fig. A2 in [16]). These results simply suggest that the quantum ground state, which is the origin of the softening, is non-magnetic.

The low-temperature softening we found in diamond (as shown in Figs. 2 and 3) is reminiscent of the elastic softening found by Goto *et al.* in their previous ultra-

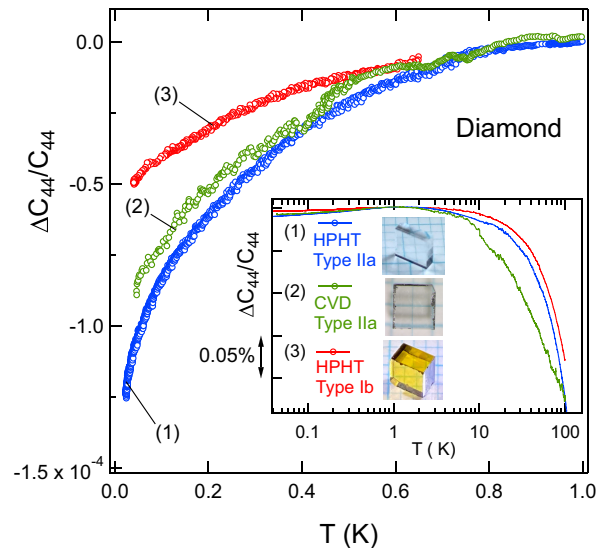


FIG. 3. Comparison of the elastic softening of C_{44} for three different types of diamond. (1: blue symbols) HPHT type IIa (see also Fig. 2), (2: green symbols) CVD type IIa, and (3: red symbols) HPHT type Ib. The relative variation in $\Delta C_{44}/C_{44}$ was normalized at 1 K (The amount of change in Sample 3 was extrapolated from 0.65 K to 1 K). The inset shows results up to 100 K in a semilogarithmic scale. Photographs of the samples used for the measurements are shown as well.

sound investigations on Si, where they successfully estimated ppb levels of V_0 vacancy concentrations in an undoped Si crystal and ppb levels of V^+ in B-doped Si grown by a floating-zone method [31–37]. In non-doped Si, the neutral vacancy V_0 has been proposed to have a 3T_1 ground state due to strong inter-orbital coupling. [38] In analogy to the interpretation for the similar softening observed in Si, it is likely that some molecular orbitals in diamond maintain a degenerate electronic state down to low temperatures, *i.e.*, the Curie-type softening of the transverse C_{44} mode (corresponding to the electric quadrupolar susceptibility of $\Gamma_5(T_2)$ symmetry [16]) in diamonds could also be connected to the T_1 or T_2 state in T_d point group.

However, the elastic softening mechanism proposed for Si [32] is unlikely to apply to diamond. In contrast, for V_0 in diamond, the electric ground state is believed to have vibronic many-body quantum states 1E and 1A_1 with a gap of 8 meV (Fig. 1(b), middle) from the various experiments on irradiated diamonds [39]. Recent ab-initio calculations [40] also demonstrate that the dynamical Jahn-Teller-distorted structure of T_d symmetry is lower in energy than the static Jahn-Teller distorted structure of D_{2d} [41], in agreement with experimental observations. Considering only the local symmetry of the low-lying vibronic quantum ground states 1E and 1A_1 , these states lack T_2 -type electric quadrupolar degrees of

TABLE I. Established electronic states of vacancy centers in diamond [27, 43]

Structure	Point Group	Electronic Config.	Ground State	Energy Gap (eV)	Refs.
V^-	T_d	$(a_1)^2(t_2)^3$	4A_2	3.150	[44]
V_0	T_d	$(a_1)^2(t_2)^2$	1E	1.674	[44]
V^+	T_d	$(a_1)^2(t_2)^1$	2T_2	$\sim 2.8^\S$	[45]
NV^-	C_{3v}	$(a_1)^2(e)^2$	3A_2	1.945	[44]
NV_0	C_{3v}	$(a_1)^2(e)^1$	2E	2.156	[46]
NV^+	C_{3v}	$(a_1)^2$	1A_1	-	[47]
BV^-	C_{3v}	$(a_1)^2(e)^2$	3A_2	-	[48]

§ theory [43]

freedom and are therefore unlikely to couple directly to the T_2 -symmetric phonon mode associated with C_{44} , *i.e.*, the doubly degenerate spin-singlet state with E symmetry cannot lead to the softening of the elastic constant C_{44} .

The alternative electronic state, 3T_1 , associated with V_0 in diamond (Fig. 1(b), right), is optically inactive and has consequently been less extensively investigated. This state possesses Γ_5 (T_2) electric quadrupolar degrees of freedom; however, it is theoretically predicted, based on perturbative calculations, to lie approximately 0.2 eV above the 1E ground state [42]. Although it may be possible that the optically inactive 3T_1 state of V_0 constitute the ground state due to strong inter-orbital coupling, analogous to the case in Si [38], this interpretation remains speculative. This theoretical framework for Si also predicts that the elastic softening persists under magnetic fields on the order of 10 T, except at ultralow temperatures, owing to the minimal lifting of orbital degeneracy via spin-orbit interaction and the orbital Zeeman effect. This is consistent with the observation that the softening in diamond, as obtained in the present study, insensitively to applied magnetic fields. (Fig. A2 in [16]) Nevertheless, the ultrasonic measurements presented here do not provide definitive evidence supporting 3T_1 as the ground state. Therefore, guided by prior theoretical insights, we conclude that the observed softening in diamond likely originates from defect states distinct from the neutral vacancy V_0 . Further experiments, such as measurements of different ultrasonic modes, investigations under higher magnetic fields, and studies with varying magnetic field orientations, are required to rigorously evaluate the potential involvement of the 3T_1 state.

In the following, we examine whether other types of known defects (as shown in Fig. 1(c)) in non-irradiated diamond could account for the observed softening. Some of the electronic ground states of the various vacancy centers in diamond are listed in Table 1. Except for the neutral vacancy V_0 , only the negatively charged vacancy V^- , and positively charged vacancy V^+ preserve T_d sym-

metry [45]. The possibility of V^+ and V^- can also be ruled out for the following reasons. Stable existence of V^+ and V^- in the crystal requires electron donors and acceptors to V_0 , which are generally provided by N and B doping, respectively. If they were the cause of the softening, it would be strongly dependent on sample, with different B and N concentrations. On the other hand, the three diamonds measured in this study have N and B concentrations that differ by an order of magnitude, but the magnitude of the softening varies much less. This fact strongly suggests that V^+ and V^- , as well as P_1 (N substitutional), B_s (B substitutional), NV and BV (N and B complex) color centers [49], are not the origin of the softening.

As shown in Table 1, the NV centers [49, 50] possess local C_{3v} symmetry due to Jahn-Teller distortion and therefore do not contribute to the elastic softening [16]. This is also true for the P_1 centers, N_nV clusters ($n = 2-4$; substitutional nitrogen atoms surrounding a vacancy), divacancies (V_2 , consisting of two adjacent missing carbon atoms), large multi-atom vacancy V_n clusters [51], and hydrogen-related complexes and other defects involving local symmetry breaking due to an asymmetric arrangement of atoms. Interactions of these defects with phonons will appear via spin-orbit coupling, which is negligible in diamond [52]. Our experimental finding that the softening is insensitive to magnetic fields further hints that nonmagnetic ground states are responsible for the softening, *i.e.*, magnetic ground states (*e.g.*, V^- , V^+ , NV^- , NV_0 , and BV^-) can be excluded as candidates. However, as mentioned above, depending on the strength of the spin-orbit interactions [38], it remains possible that even for a magnetic state such as spin-triplet 3T_1 , the magnetic field response could be sufficiently weak within the measured field and temperature ranges. Thus, we cannot definitively rule out all magnetic ground states with finite spin.

Although the known defects discussed above have been ruled out as the origin of the softening, non-irradiated diamond may still host as-yet-unidentified vacancies or interstitials that preserve local T_d symmetry. Their quantum ground states likely remain optically inactive or undetermined, and could account for the observed elastic softening. The possible physical picture envisaged here is a situation where the orbitally degenerated multi-electronic state of T_1 or T_2 is coupled to the T_2 -phonon mode, and forming a vibronic state due to the dynamical Jahn-Teller effect. It will allow the system to preserve tetrahedral symmetry without causing static Jahn-Teller distortion, similar to the quantum tunneling state in the cubic clathrate crystals [53]. Another example is the cubic, non-Kramers Γ_3 ground state system of PrMg_3 , which has no long-range order down to 50 mK, where a quantum-mechanical hybridization of $4f$ electrons and phonons is believed to form the vibronic state. [54]. To clarify the origin of the softening, it would be desirable

to compare irradiated and non-irradiated samples, and to perform similar measurements on samples with controlled impurity profiles including dislocations and elongation defects while systematically varying the concentrations of nitrogen, boron, carbon vacancies, and other relevant impurities. This represents a challenge for future investigations.

Finally, we follow the phenomenological analysis of quadrupolar susceptibility. The solid red line in Fig. 2(a) is the result of calculations based on the equation $C_{\Gamma_5} = C_{\Gamma_5}^{bk}(T - T_C)/(T - \Theta)$ (for details, see [16]). The fit yields $T_C = -260.196$ mK, $\Theta = -260.242$ mK, and the Jahn-Teller energy $\Delta_{JT} = T_C - \Theta = 0.046$ mK. The dashed line represents the phenomenological fit for the background contribution $C_{\Gamma_5}^{bk} = C_{\Gamma_5}^0 - s/\{\exp(t/T) - 1\}$ [25], with $C_{\Gamma_5}^0 = 5.69923 \times 10^{11}$ Jm⁻³, $s = -4.681226 \times 10^7$ Jm⁻³, and $t = 2.941652$ K. The negative value of Θ indicates antiferro-type inter-site interactions for the electric quadrupole on the unspecified defect. The negative value of T_C suggests quadrupolar fluctuations associated with the degenerate ground state even at the lowest temperature of ~ 20 mK. This result further proves that the cubic site symmetry T_d at the site of defects that cause softening is preserved in the investigated diamond material, *i.e.*, the local distortion owing to the static Jahn-Teller effect is irrelevant for diamond with low vacancy and impurity concentrations. If we roughly estimate the concentration of the unspecified defects which have electric quadrupole degrees of freedom using the relation $N = \Delta_{JT}C_{\Gamma}^0/(\delta_{\Gamma}^0)^2$ for the acoustic mode C_{44} , which is assuming a T_2 -triplet ground state and was used to analyze the vacancy concentration in Si [32]. Here, N denotes the concentration and δ_{Γ}^0 the deformation binding energy of unspecified defect. As a rough estimation, we assume the formation energy 9–15 eV of the vacancies in diamond [55], then we obtain the concentration $N \sim 0.98 - 0.36$ ppb. If the unspecified defects possess similar formation energies, this would imply that all diamonds examined in this study host defects with electric quadrupole moments on the order of ppb.

In summary, we performed ultrasonic measurements down to 20 mK on non-irradiated synthetic diamonds and discovered anomalous elastic softening. Although the origin of this softening remains unresolved, this result suggests the presence of an unspecified defect-derived quantum ground state with T_1 or T_2 symmetry in synthetic diamonds. Our phenomenological analysis implies that the concentration of the defect is at the ppb level. The present results are particularly relevant for researchers employing synthetic diamonds in diverse fields, including quantum information, biological sensing, and power electronics. Moreover, our findings offer a new avenue for exploring the quantum ground states of vacancies in diamond. Further studies of the elastic response of various diamond types at cryogenic temperatures are essential to elucidate the underlying

physics of diamond vacancies and defects, with potential implications for future technological applications.

We thank Profs. Terutaka Goto, Takashi Taniguchi, Hiroaki Kusunose, and Satoru Hayami for helpful discussions. The present research was supported by JSPS KAKENHI Grants Nos. JP23H04868, JP21KK0046, JP22K03501, and Toyota Physical and Chemical Research Institute under the 2021 Toyota Riken Scholar Collaborative Research Program (Phase 1) to TY and TT. We acknowledge support from the DFG through the Würzburg-Dresden Cluster of Excellence on Complexity and Topology in Quantum Matter - *ct.qmat* (EXC 2147, project-id 390858490) and from the HLD at HZDR, a member of the European Magnetic Field Laboratory (EMFL). TY would like to acknowledge Mr. Kousuke Nakamura and Mr. Tatsuji Meike at Hokkaido University Technical Support Division for assistance in polishing the diamonds. TY and RH would like to thank Prof. Atsuhiko Miyata for supporting the measurements at HZDR.

-
- [1] M. Kasu, N. C. Saha, T. Oishi, and S.-W. Kim, Fabrication of diamond modulation-doped FETs by NO₂ delta doping in an Al₂O₃ gate layer, *Appl. Phys. Exp.* **14**, 051004 (2021).
 - [2] A. M. Zaitsev, *Optical Properties of Diamond* (Springer Berlin Heidelberg, 2001).
 - [3] R. S. Balmer, J. R. Brandon, S. L. Clewes, H. K. Dhillon, J. M. Dodson, I. Friel, P. N. Inglis, T. D. Madgwick, M. L. Markham, T. P. Mollart, N. Perkins, G. A. Scarsbrook, D. J. Twitchen, A. J. Whitehead, J. J. Wilman, and S. M. Woollard, Chemical vapour deposition synthetic diamond: materials, technology and applications, *J. Phys.: Cond. Matter* **21**, 364221 (2009).
 - [4] H. Sumiya, K. Harano, and K. Tamasaku, HPHT synthesis and crystalline quality of large high-quality (001) and (111) diamond crystals, *Dia. Rel. Mater.* **58**, 221 (2015).
 - [5] S. Eaton-Magaña and J. E. Shigley, Observations on CVD-grown synthetic diamonds: A Review, *Gems and Gemology* **52**, 222 (2016).
 - [6] V. Acosta and P. Hemmer, Nitrogen-vacancy centers: Physics and applications, *MRS Bulletin* **38**, 127 (2013).
 - [7] D. R. Glenn, K. Lee, H. Park, R. Weissleder, A. Yacoby, M. D. Lukin, H. Lee, R. L. Walsworth, and C. B. Connolly, Single-cell magnetic imaging using a quantum diamond microscope, *Nat. Meth.* **12**, 736 (2015).
 - [8] H. Morishita, T. Tashima, D. Mima, H. Kato, T. Makino, S. Yamasaki, M. Fujiwara, and N. Mizuochi, Extension of the Coherence Time by Generating MW Dressed States in a Single NV Centre in Diamond, *Sci. Rep.* **9**, 13318 (2019).
 - [9] J. F. Barry, J. M. Schloss, E. Bauch, M. J. Turner, C. A. Hart, L. M. Pham, and R. L. Walsworth, Sensitivity optimization for NV-diamond magnetometry, *Rev. Mod. Phys.* **92**, 015004 (2020).
 - [10] B. Hensen, H. Bernien, A. E. Dréau, A. Reiserer, N. Kalb,

- M. S. Blok, J. Ruitenbergh, R. F. L. Vermeulen, R. N. Schouten, C. Abellán, W. Amaya, V. Pruneri, M. W. Mitchell, M. Markham, D. J. Twitchen, D. Elkouss, S. Wehner, T. H. Taminiau, and R. Hanson, Loophole-free Bell inequality violation using electron spins separated by 1.3 kilometres, *Nature* **526**, 682 (2015).
- [11] T. Tashima, H. Morishita, and N. Mizuochi, Experimental demonstration of two-photon magnetic resonances in a single-spin system of a solid, *Phys. Rev. A* **100**, 023801 (2019).
- [12] K. S. Cujia, J. M. Boss, K. Herb, J. Zopes, and C. L. Degen, Tracking the precession of single nuclear spins by weak measurements, *Nature* **571**, 230 (2019).
- [13] L. Childress and R. Hanson, Diamond NV centers for quantum computing and quantum networks, *MRS Bulletin* **38**, 134 (2013).
- [14] T. Nakazato, R. Reyes, N. Imaike, K. Matsuda, K. Tsurumoto, Y. Sekiguchi, and H. Kosaka, Quantum error correction of spin quantum memories in diamond under a zero magnetic field, *Commun. Phys.* **5**, 102 (2022).
- [15] F. Rozpedek, R. Yehia, K. Goodenough, M. Ruf, P. C. Humphreys, R. Hanson, S. Wehner, and D. Elkouss, Near-term quantum-repeater experiments with nitrogen-vacancy centers: Overcoming the limitations of direct transmission, *Phys. Rev. A* **99**, 052330 (2019).
- [16] See Supplemental Material for (1) Thermodynamic Consideration of the Formation of Atomic Vacancies, (2) Ultrasonic Method, (3) Wavefunctions for sp^3 Hybrid Orbitals and Active Electric Quadrupoles, (4) Quadrupolar Susceptibility, (5) Comparison of Si and Diamond, and (6) Magnetic Field Dependence of the Softening of C_{44} , and (7) Effects of NV^- , NV_0 , and nuclear spins.
- [17] K. V. Bogdanov, M. V. Zhukovskaya, V. Y. Osipov, E. V. Ushakova, M. A. Baranov, K. Takai, A. Rampersaud, and A. V. Baranov, Highly intensive emission of the NV^- centers in synthetic HPHT microdiamonds at low nitrogen doping, *APL Materials* **6**, 086104 (2018).
- [18] A. Stoneham, The low-lying levels of the GR 1 centre in diamond, *Solid State Commun.* **21**, 339 (1977).
- [19] S. Subedi, V. Fedorov, S. Mirov, and M. Markham, Spectroscopy of GR1 centers in synthetic diamonds, *Opt. Mater. Exp.* **11**, 757 (2021).
- [20] S. Pezzagna, D. Rogalla, D. Wildanger, J. Meijer, and A. Zaitsev, Creation and nature of optical centres in diamond for single-photon emission—overview and critical remarks, *New J. Phys.* **13**, 035024 (2011).
- [21] T. Lühmann, N. Raatz, R. John, M. Lesik, J. Rödiger, M. Portail, D. Wildanger, F. Kleißler, K. Nordlund, A. Zaitsev, J.-F. Roch, A. Tallaire, J. Meijer, and S. Pezzagna, Screening and engineering of colour centres in diamond, *J. Phys. D: Appl. Phys.* **51**, 483002 (2018).
- [22] H. Sumikura, K. Hirama, K. Nishiguchi, A. Shinya, and M. Notomi, Highly nitrogen-vacancy doped diamond nanostructures fabricated by ion implantation and optimum annealing, *APL Materials* **8**, 031113 (2020).
- [23] T. Luo, L. Lindner, J. Langer, V. Cimalla, X. Vidal, F. Hahl, C. Schreyvogel, S. Onoda, S. Ishii, T. Ohshima, D. Wang, D. A. Simpson, B. C. Johnson, M. Capelli, R. Blinder, and J. Jeske, Creation of nitrogen-vacancy centers in chemical vapor deposition diamond for sensing applications, *New J. Phys.* **27**, 033030 (2022).
- [24] *Handbook of Scientific Tables* (World Scientific, 2022).
- [25] B. Lüthi, *Physical Acoustics in the Solid State* (Springer, Berlin, 2006).
- [26] C. A. Coulson and M. J. Kearsley, Colour centres in irradiated diamonds. I, *Proc. Royal Soc. Lond. A* **241**, 433 (1957).
- [27] G. Davies, The Jahn-Teller effect and vibronic coupling at deep levels in diamond, *Rep. Prog. Phys.* **44**, 787 (1981).
- [28] H. J. McSkimin and P. Andreatch, Elastic Moduli of Diamond as a Function of Pressure and Temperature, *J. Appl. Phys.* **43**, 2944 (1972).
- [29] A. Migliori, H. Ledbetter, R. G. Leisure, C. Pantea, and J. B. Betts, Diamond's elastic stiffnesses from 322 K to 10 K, *J. Appl. Phys.* **104**, 053512 (2008).
- [30] A. Nagakubo, M. Arita, H. Ogi, H. Sumiya, N. Nakamura, and M. Hirao, Elastic constant C_{11} of ^{12}C diamond between 10 and 613 K, *Appl. Phys. Lett.* **108**, 221902 (2016).
- [31] H. Yamada-Kaneta, T. Goto, Y. Saito, Y. Nemoto, K. Sato, K. Kakimoto, and S. Nakamura, Vacancies in defect-free zone of point-defect-controlled CZ silicon observed by low-temperature ultrasonic measurements, *Mater. Sci. and Eng.: B* **134**, 240 (2006).
- [32] T. Goto, H. Yamada-Kaneta, Y. Saito, Y. Nemoto, K. Sato, K. Kakimoto, and S. Nakamura, Observation of Low-Temperature Elastic Softening due to Vacancy in Crystalline Silicon, *J. Phys. Soc. Jpn.* **75**, 044602 (2006).
- [33] T. Goto, K. Mitsumoto, M. Akatsu, S. Baba, K. Okabe, R. Takasu, Y. Nemoto, H. Yamada-Kaneta, Y. Furumura, H. Saito, K. Kashima, and Y. Saito, Surface acoustic wave diagnosis of vacancy orbital with electric quadrupoles in silicon, *J. Phys.: Conf. Ser.* **592**, 012150 (2015).
- [34] K. Okabe, M. Akatsu, S. Baba, K. Mitsumoto, Y. Nemoto, H. Yamada-Kaneta, T. Goto, H. Saito, K. Kashima, and Y. Saito, Strong Quadrupole-Strain Interaction of Vacancy Orbital in Boron-Doped Czochralski Silicon, *J. Phys. Soc. Jpn.* **82**, 124604 (2013).
- [35] K. Mitsumoto, M. Akatsu, S. Baba, R. Takasu, Y. Nemoto, T. Goto, H. Yamada-Kaneta, Y. Furumura, H. Saito, K. Kashima, and Y. Saito, Elastic Softening of Surface Acoustic Wave Caused by Vacancy Orbital in Silicon Wafer, *J. Phys. Soc. Jpn.* **83**, 034702 (2014).
- [36] S. Baba, T. Goto, Y. Nagai, M. Akatsu, H. Watanabe, K. Mitsumoto, T. Ogawa, Y. Nemoto, and H. Yamada-Kaneta, Quadrupole Effects of Vacancy Orbital in Boron-Doped Silicon, *J. Phys. Soc. Jpn.* **80**, 094601 (2011).
- [37] T. Goto, H. Yamada-Kaneta, K. Sato, M. Hikin, Y. Nemoto, and S. Nakamura, Observation of vacancy in crystalline silicon using low-temperature ultrasonic measurements, *Physica B* **401-402**, 109 (2007).
- [38] H. Matsuura and K. Miyake, Theory on softening of elastic constants in non-doped and b-doped si with a vacancy, *J. Phys. Soc. Jpn.* **77**, 043601 (2008).
- [39] G. Davies, ed., *Properties and growth of diamond*, EMIS datareviews series 9 (INSPEC, 1994).
- [40] J. C. A. Prentice, B. Monserrat, and R. J. Needs, First-principles study of the dynamic Jahn-Teller distortion of the neutral vacancy in diamond, *Phys. Rev. B* **95**, 014108 (2017).
- [41] C. Clark and J. Walker, The neutral vacancy in diamond, *Proc. Royal Soc. Lond. A* **334**, 241 (1973).
- [42] J. A. van Wyk, O. D. Tucker, M. E. Newton, J. M. Baker, G. S. Woods, and P. Spear, Magnetic-resonance measurements on the $^5\text{A}_2$ excited state of the neutral vacancy in

- diamond, *Phys. Rev. B* **52**, 12657 (1995).
- [43] A. Mainwood and A. M. Stoneham, Stability of electronic states of the vacancy in diamond, *J. Phys.: Cond. Matt.* **9**, 2453 (1997).
- [44] G. Davies, S. C. Lawson, A. T. Collins, A. Mainwood, and S. J. Sharp, Vacancy-related centers in diamond, *Phys. Rev. B* **46**, 13157 (1992).
- [45] C. Coulson and F. Larkins, Isolated single vacancy in diamond—I. Electronic structure, *J. Phys. Chem. Solids* **32**, 2245 (1971).
- [46] P. Siyushev, H. Pinto, M. Vörös, A. Gali, F. Jelezko, and J. Wrachtrup, Optically Controlled Switching of the Charge State of a Single Nitrogen-Vacancy Center in Diamond at Cryogenic Temperatures, *Phys. Rev. Lett.* **110**, 167402 (2013).
- [47] C. J. Meara, M. J. Rayson, P. R. Briddon, and J. P. Goss, Density functional theory study on magnetically detecting positively charged nitrogen-vacancy center in diamond, *Phys. Rev. B* **100**, 104108 (2019).
- [48] T. Umeda, K. Watanabe, H. Hara, H. Sumiya, S. Onoda, A. Uedono, I. Chuprina, P. Siyushev, F. Jelezko, J. Wrachtrup, and J. Isoya, Negatively charged boron vacancy center in diamond, *Phys. Rev. B* **105**, 165201 (2022).
- [49] A. Cox, M. E. Newton, and J. M. Baker, ^{13}C , ^{14}N and ^{15}N ENDOR measurements on the single substitutional nitrogen centre (P1) in diamond, *J. Phys.: Cond. Matt.* **6**, 551 (1994).
- [50] M. W. Doherty, N. B. Manson, P. Delaney, F. Jelezko, J. Wrachtrup, and L. C. Hollenberg, The nitrogen-vacancy colour centre in diamond, *Phys. Rep.* **528**, 1 (2013).
- [51] D. Kamihara, T. Shimizu, and K. Uchida, Discovery of Peculiar Electronic Structures of Decavacancy V_{10} in Silicon Crystal, *J. Phys. Soc. Jpn.* **91**, 064709 (2022).
- [52] A. Lenef and S. C. Rand, Electronic structure of the N-V center in diamond: Theory, *Phys. Rev. B* **53**, 13441 (1996).
- [53] T. Goto, Y. Nemoto, T. Yamaguchi, M. Akatsu, and T. Yanagisawa, Tunneling and rattling in clathrate crystal, *Phys. Rev. B* **70**, 184126 (2004).
- [54] K. Araki, T. Goto, K. Mitsumoto, Y. Nemoto, M. Akatsu, H. S. Suzuki, H. Tanida, S. Takagi, S. Yasin, S. Zherlitsyn, and J. Wosnitza, Dissipation in Non-Kramers Doublet of PrMg_3 , *J. Phys. Soc. Jpn.* **81**, 023710 (2012).
- [55] J. C. Bourgoin, An experimental estimation of the vacancy formation energy in diamond, *Radiation Effects* **79**, 235 (1983).

Supplemental Material for Elastic Softening in Synthetic Diamonds

Tatsuya Yanagisawa, Ruo Hibino, Hiroyuki Hidaka, Hiroshi Amitsuka, Toshiyuki Tashima, Mitsuhiro Akatsu, Yuichi Nemoto, Sergei Zherlitsyn, and Joachim Wosnitza

1. THERMODYNAMIC CONSIDERATIONS OF THE FORMATION OF ATOMIC VACANCIES

Point defects are always formed during crystal growth at high temperatures. In other words, it is thermodynamically inevitable that such structural instability exists even in thermal equilibrium because there is always finite entropy at a finite temperature, according to the laws of thermodynamics. If N point defects (single-electron vacancies) form in a crystal consisting of N_0 atoms and assuming that $N \ll N_0$ and the formation energy of a single atomic vacancy is E_V , then Gibbs's free energy is written by,

$$\Delta G = \Delta U - T\Delta S = NE_V - T\Delta S, \quad (1)$$

where the entropy is $S = -k_B \ln W$, with the number of states $W = \frac{N!}{(N_0 - N)N!}$.

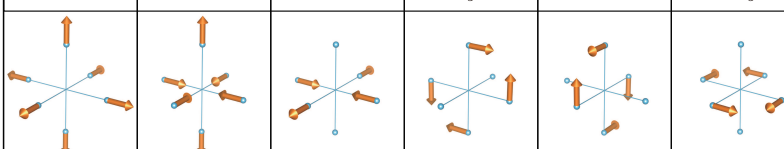
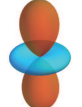
From the approximation by Stirling's formula with $N \gg 1$, the entropy can be rewritten as follows,

$$\Delta S = -k_B N \left\{ \frac{N_0}{N} \ln \frac{N_0}{N} - \frac{(N_0 - N)}{N} \ln \frac{(N_0 - N)}{N} \right\}. \quad (2)$$

Substituting this for $\frac{dS}{dE} = \frac{1}{T}$, we obtain the temperature dependence of the number of atomic vacancies $N = N_0 e^{(-E_V/T)}$. Although the atomic vacancy-formation energy is unknown, this equation shows that the number of atomic vacancies increases rapidly during crystal growth with increasing temperatures.

2. ULTRASONIC METHOD

TABLE AI: Symmetry, elastic constant, symmetrized strain and quadrupole, and illustration of strain and coupled charge distributions.

Symmetry	$\Gamma_1(A_{1g})$	$\Gamma_3(E_g)$		$\Gamma_5(T_{2g})$		
Elastic Const.	C_B	$(C_{11} - C_{12})/2$		C_{44}		
Symmetrized Strains	ε_B	ε_u	ε_v	ε_{yz}	ε_{zx}	ε_{xy}
						
Stevens Op.	O_B	O_2^0	O_2^2	O_{yz}	O_{zx}	O_{xy}

Ultrasonic measurements have been widely used in studies of solid-state physics. They are valuable tools for detailed characterization of the lattice elasticity as well as any other type of phenomenon that couple to the strain fields. Some examples are phenomena involving electric quadrupolar degrees of freedom, magnetic ordering (via exchange-striction coupling), superconductivity, local Einstein phonons, magneto-acoustic quantum oscillations, and so on [25]. By using longitudinal and transverse ultrasonic modes, the response of these phenomena can be obtained spectroscopically. In particular, the temperature dependence of the elastic constant is one of the powerful tools to investigate the quadrupolar degrees of freedom in the sp^3 dangling bond of the single neutral vacancy V_0 in Si and diamond. The Γ_5 -type symmetrized elastic strains ϵ_{yz} , ϵ_{zx} , and ϵ_{xy} , that correspond to the C_{44} transverse ultrasonic modes, couple to the electric quadrupole with the same symmetry as O_{yz} , O_{zx} , and O_{xy} , which are active in the quantum ground state.

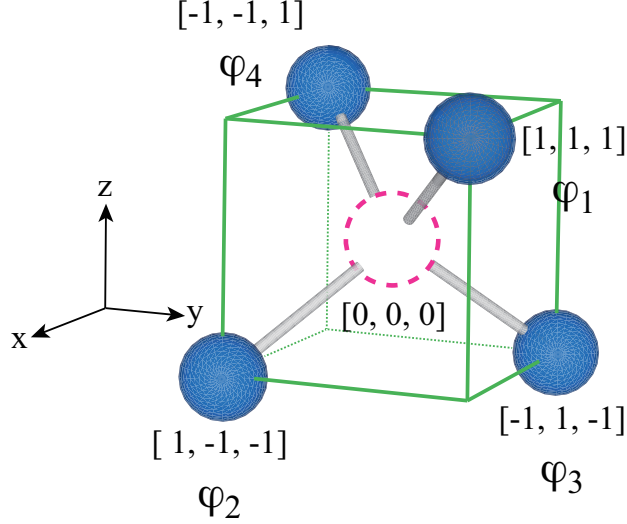


FIG. A1 Scheme of the dangling bonds of a single atomic vacancy.

3. WAVEFUNCTIONS FOR sp^3 HYBRID ORBITALS AND ACTIVE ELECTRIC QUADRUPOLES

Diamond is covalently bonded by the four outer-shell carbon $2s^1 2p^3$ electrons, forming hybridized orbitals. As shown in Fig. A1, when the dangling bonds of carbon atoms in the direct neighborhood of a single-atom vacancy are numbered from 1 to 4, the wave functions of the dangling bonds are given by,

$$\begin{aligned}
 \phi_1 &= \frac{1}{2}(s^{(1)} + p_x^{(1)} + p_y^{(1)} + p_z^{(1)}), \\
 \phi_2 &= \frac{1}{2}(s^{(1)} + p_x^{(1)} - p_y^{(1)} - p_z^{(1)}), \\
 \phi_3 &= \frac{1}{2}(s^{(1)} - p_x^{(1)} + p_y^{(1)} - p_z^{(1)}), \\
 \phi_4 &= \frac{1}{2}(s^{(1)} + p_x^{(1)} - p_y^{(1)} + p_z^{(1)}).
 \end{aligned} \tag{3}$$

These equations represent the four-fold degeneracy of equivalent sp^3 hybrid orbitals. The transfer energy among the sp^3 dangling bonds is written as, $-\gamma = \langle \phi_j | \mathcal{H}_0 | \phi_i \rangle$ ($i, j = 1, 2, 3$, and 4). Here, the Hamiltonian H_0 for the transfer motions among the dangling bonds has cubic symmetry. When we assume the energy of the dangling bonds is E , the matrix elements of H_0 are written as,

$$\mathcal{H}_0 = \begin{array}{c} \langle \phi_1 | \\ \langle \phi_2 | \\ \langle \phi_3 | \\ \langle \phi_4 | \end{array} \begin{array}{cccc} | \phi_1 \rangle & | \phi_2 \rangle & | \phi_3 \rangle & | \phi_4 \rangle \\ E & -\gamma & -\gamma & -\gamma \\ -\gamma & E & -\gamma & -\gamma \\ -\gamma & -\gamma & E & -\gamma \\ -\gamma & -\gamma & -\gamma & E \end{array} \tag{4}$$

By diagonalizing Eq. (4), we obtain

$$\mathcal{H}_0 = \begin{array}{c|cccc} & |\psi^{a1}\rangle & |\psi^{a2}\rangle & |\psi^{a3}\rangle & |\psi^{a4}\rangle \\ \langle\psi^{a1}| & E - 3\gamma & 0 & 0 & 0 \\ \langle\psi^{a2}| & 0 & E + \gamma & 0 & 0 \\ \langle\psi^{a3}| & 0 & 0 & E + \gamma & 0 \\ \langle\psi^{a4}| & 0 & 0 & 0 & E + \gamma \end{array} \quad (5)$$

This shows that the ground state is a singlet and the excited state splits into a triplet with an energy difference of 4γ under the site symmetry T_d . The single-electron wavefunctions of the eigenstates are

$$\begin{aligned} a_1 : |\psi^{(a1)}\rangle &= |v\rangle = \frac{1}{2}(|\phi_1\rangle + |\phi_2\rangle + |\phi_3\rangle + |\phi_4\rangle) \\ t_2 : \begin{cases} |\psi_a^{(t2)}\rangle &= |a\rangle = \frac{1}{2}(|\phi_1\rangle + |\phi_2\rangle - |\phi_3\rangle - |\phi_4\rangle) \\ |\psi_b^{(t2)}\rangle &= |b\rangle = \frac{1}{2}(|\phi_1\rangle - |\phi_2\rangle + |\phi_3\rangle - |\phi_4\rangle) \\ |\psi_c^{(t2)}\rangle &= |c\rangle = \frac{1}{2}(|\phi_1\rangle - |\phi_2\rangle - |\phi_3\rangle + |\phi_4\rangle) \end{cases} \end{aligned} \quad (6)$$

We use the notations related to the irreducible representations A , E , and T for the symmetry of the system (quantum ground state), and labels a , e , and t_2 for the individual electron orbitals. The expression for the degrees of freedom that the excited triplet of the dangling orbitals have in the direct product space is

$$(t_2 \otimes t_2) = A \oplus E \oplus T_1 \oplus T_2. \quad (7)$$

Goto *et al.* consider the orbital part of T_2 state in this product space to be the cause of the softening of Si and conduct a phenomenological analysis. [32] Actually, the electronic state of the neutral vacancy V_0 has two electrons in the excited triplet t_2 , which is the electron configuration of $(a_1^2 t_2^2)$. Thus, it is important to consider multi-electron states including Pauli's exclusion rule for spin degrees of freedom, which can be decomposed into [26]

$${}^1A_1 \oplus {}^1E \oplus {}^3T_1 \oplus {}^1T_2. \quad (8)$$

For neutral vacancy V_0 in diamond, it is both theoretically and experimentally confirmed that 1E is the ground state. [39?] On the other hand, for the neutral vacancy V_0 in non-doped Si, it is proposed from theoretical calculations that 3T_1 could be the ground state due to strong inter-orbital interactions. [38]

The wavefunctions for the each state of the electron configuration of $(a_1^2 t_2^2)$ are expressed in a simplified form as follows,

$$\begin{aligned} {}^1A_1 : & (|v\bar{v}a\bar{a}\rangle + |v\bar{v}b\bar{b}\rangle + |v\bar{v}c\bar{c}\rangle) \\ {}^1E : & (|v\bar{v}a\bar{a}\rangle - |v\bar{v}b\bar{b}\rangle) \\ {}^1T_2 : & (|v\bar{v}a\bar{b}\rangle - |v\bar{v}a\bar{b}\rangle) \\ {}^3T_1 : & (|v\bar{v}ab\rangle) \end{aligned} \quad (9)$$

Here, the wavefunctions are unnormalized. The bars above orbital denote spin states, and only those with $S_z = S$ are shown. For each degenerate representation, only a single component is presented. [26]

The product space of the triplet states are

$$T_1 \otimes T_1 = T_2 \otimes T_2 = A_1 \oplus A_2 \oplus E \oplus T_1 \oplus T_2. \quad (10)$$

Thus, both triplet state possess active electric quadrupole with $\Gamma_3(E)$ and $\Gamma_5(T_2)$ symmetries.

Here, we introduce the Gell-Mann matrices λ_i ($i = 1, 2, \dots, 8$) of the generator of the rotation group $SU(3)$ representing the active electric quadrupoles with $\Gamma_3(E)$ and $\Gamma_5(T_2)$ symmetries as follows,

$$\begin{aligned}
&\Gamma_3(E) : \\
&O_u = \lambda_8 = \frac{1}{\sqrt{3}} \begin{pmatrix} 1 & 0 & 0 \\ 0 & 1 & 0 \\ 0 & 0 & -2 \end{pmatrix} \\
&O_v = \lambda_1 = \frac{1}{\sqrt{3}} \begin{pmatrix} 0 & 1 & 0 \\ 1 & 0 & 0 \\ 0 & 0 & 0 \end{pmatrix}
\end{aligned} \tag{11}$$

$$\begin{aligned}
&\Gamma_5(T_2) : \\
&O_{yz} = \frac{1}{\sqrt{2}}(\lambda_5 - \lambda_7) = \frac{1}{\sqrt{2}} \begin{pmatrix} 0 & 0 & -i \\ 0 & 0 & i \\ i & -i & 0 \end{pmatrix} \\
&O_{zx} = \frac{1}{\sqrt{2}}(\lambda_4 + \lambda_6) = \frac{1}{\sqrt{2}} \begin{pmatrix} 0 & 0 & 1 \\ 0 & 0 & 1 \\ 1 & 1 & 0 \end{pmatrix} \\
&O_{xy} = -\lambda_2 = \frac{1}{\sqrt{2}} \begin{pmatrix} 0 & i & 0 \\ -i & 0 & 0 \\ 0 & 0 & 0 \end{pmatrix}
\end{aligned} \tag{12}$$

When the local charge fluctuations of the charge state of the vacancy site is denoted by Q_Γ , it is connected to the quadrupole operator obtained above by the relation:

$$Q_\Gamma = Z^* a^{*2} O_\Gamma. \tag{13}$$

Here, Z^* is the effective charge and a^* is the effective radius of the quadrupole with symmetry Γ .

4. QUADRUPOLAR SUSCEPTIBILITY

The temperature dependence of the elastic constant in the present paper is calculated using a theory based on the Wigner-Brillouin perturbation method. The crystalline electric field (CEF) Hamiltonian with electric-strain-mediated perturbation is

$$\mathcal{H} = \mathcal{H}_0 + \sum_{\Gamma} \frac{\partial \mathcal{H}_0}{\partial \epsilon_\Gamma} \epsilon_\Gamma. \tag{14}$$

Here, \mathcal{H}_0 is derived from the electrostatic potential in the absence of strain ϵ_Γ . The second term in Eq. (14) is given in terms of electric quadrupole-strain interaction. To describe the elastic softening in C_{44} , we adopt the quadrupole-strain interaction regarding Γ_3 and Γ_5 symmetry as

$$\begin{aligned}
\mathcal{H}_{\text{QS}} &= -g_{\Gamma_3} O_{\Gamma_3} \epsilon_{\Gamma_3} - g_{\Gamma_5} O_{\Gamma_5} \epsilon_{\Gamma_5} \\
&= -g_{\Gamma_3} (O_u \epsilon_u + O_v \epsilon_v) - g_{\Gamma_5} (O_{yz} \epsilon_{yz} + O_{zx} \epsilon_{zx} + O_{xy} \epsilon_{xy}),
\end{aligned} \tag{15}$$

where g_Γ is a coupling constants, and O_Γ is an electric quadrupolar moment (as listed in Table AI).

Here, g_{Γ_3} and g_{Γ_5} are coupling constant. O_{Γ_3} and O_{Γ_5} are the electric quadrupoles belonging to the Γ_3 and Γ_5 symmetries, respectively, as defined in the previous section. In the ultrasonic experiments, the symmetrized strain ϵ_Γ is induced by ultrasound. The quadrupole-strain interaction is incorporated as a perturbed crystal-field level $E_i(\epsilon_\Gamma)$ as a function of symmetrized strain, and we consider strain up to second-order perturbation. The crystal-field energy can be written as:

$$\begin{aligned}
E_i(\epsilon_\Gamma) &= E_i^0 - \langle i | \mathcal{H}_{QS} | i \rangle + \sum_{j \neq i} \frac{|\langle j | \mathcal{H}_{QS} | i \rangle|^2}{E_j^{(0)} - E_i^{(0)}} \\
&= E_i^0 + g_\Gamma \epsilon_\Gamma \langle i | O_\Gamma | i \rangle + g_\Gamma^2 \epsilon_\Gamma^2 \sum_{j \neq i} \frac{|\langle j | O_\Gamma | i \rangle|^2}{E_j^{(0)} - E_i^{(0)}}
\end{aligned} \tag{16}$$

where E_i is the energy in the quantum state $|i\rangle$. The total free energy F in a crystal is the sum of the elastic energy and the free energy of the electronic system,

$$F = \frac{1}{2} \sum_{\Gamma} C_\Gamma^{(0)} \epsilon_\Gamma^2 - N k_B T \ln \sum_i \exp\{-E_i(\epsilon_\Gamma)/k_B T\}, \tag{17}$$

where $C_\Gamma^{(0)}$ is the elastic constant without quadrupole-strain interaction, and N is the number of electric quadrupoles, *i.e.*, single atomic vacancies, per unit volume in the case of Si. The elastic constant $C_\Gamma(T)$ is obtained by the second derivative of the Helmholtz free energy F with respect to strain in the limit $\epsilon_\Gamma \rightarrow 0$.

$$C_\Gamma(T) = \left(\frac{\partial^2 F}{\partial \epsilon_\Gamma^2} \right)_{\epsilon_\Gamma \rightarrow 0} = C_\Gamma^0 - N g_\Gamma^2 \chi_\Gamma(T), \tag{18}$$

$$-g_\Gamma^2 \chi_\Gamma = \left\langle \frac{\partial^2 E_i}{\partial \epsilon_\Gamma^2} \right\rangle - \frac{1}{k_B T} \left[\left\langle \left(\frac{\partial E_i}{\partial \epsilon_\Gamma} \right)^2 \right\rangle - \left\langle \frac{\partial E_i}{\partial \epsilon_\Gamma} \right\rangle^2 \right], \tag{19}$$

where $\chi_\Gamma(T)$ is the quadrupolar susceptibility of Γ symmetry. In addition to the strain-quadrupole interaction, inter-site quadrupole-quadrupole interactions are considered. Here, we focus on the k site. Quadrupoles other than the k site are taken into account by mean-field approximation,

$$\mathcal{H}_{QQ(\Gamma)}^{MF} = - \sum_k g'_\Gamma \langle O_\Gamma \rangle O_\Gamma^{(k)}, \tag{20}$$

and the Hamiltonian of the system can be written as:

$$\begin{aligned}
\mathcal{H} &= \mathcal{H}_0 + \mathcal{H}_{QS} + \mathcal{H}_{QQ}^{MF} \\
&= -g_\Gamma \sum_k \sum_\Gamma O_\Gamma^{(k)} \epsilon_\Gamma^{eff}.
\end{aligned} \tag{21}$$

$\epsilon_\Gamma^{eff} = \epsilon_\Gamma + \frac{g'_\Gamma}{g_\Gamma} \langle O_\Gamma \rangle$ is the effective mean-field strain. The elastic constants [Eq. (18)], including inter-site interactions, are rewritten as:

$$C_\Gamma(T) = C_\Gamma^0 - \frac{N g_\Gamma^2 \chi_\Gamma(T)}{1 - g'_\Gamma \chi_\Gamma(T)}. \tag{22}$$

The second-order perturbation term in the energy [the third term on the right-hand side of Eq. (16)], and the so-called van Vleck term in the quadrupolar susceptibility [the first term on the right-hand side of Eq. (19)] should also be addressed. In first-order perturbation, the thermal average due to strain is zero. So, only the Curie term, which is inversely proportional to T , appears in the quadrupolar susceptibility,

$$-g_\Gamma^2 \chi_\Gamma = -\frac{1}{k_B T} \left[\left\langle \left(\frac{\partial E_i}{\partial \epsilon_\Gamma} \right)^2 \right\rangle - \left\langle \frac{\partial E_i}{\partial \epsilon_\Gamma} \right\rangle^2 \right]. \tag{23}$$

Diagonalizing the quadrupole operators with Γ symmetry in Eq. (13) and calculating the quadrupolar susceptibility with Γ symmetry in Eqs. (14) to (22), we obtain,

$$-g_{\Gamma}^2 \chi_{\Gamma} = -\frac{2g_{\Gamma}^2}{3k_B T}. \quad (24)$$

Substituting Eq. (24) into Eq. (22) yields

$$C_{\Gamma}(T) = C_{\Gamma}^{(0)} \left(\frac{T - T_C}{T - \Theta} \right). \quad (25)$$

Here, $\Theta = \frac{2g'_{\Gamma}}{3k_B}$ is the coupling constant of the quadrupole-quadrupole interaction. T_C is the total energy of the quadrupolar interaction, which is described as $T_C = \Theta + \Delta_{JT}$, with the binding energy of the strain field between quadrupoles $\Delta_{JT} = T_C - \Theta = \frac{2Ng_{\Gamma}^2}{3k_B C_{\Gamma}^{(0)}}$, *i.e.*, the so-called Jahn-Teller energy. Using the transformational binding energy $\delta_{\Gamma} = \sqrt{\frac{2}{3}}g_{\Gamma}$, the quadrupole susceptibility can be rewritten as

$$\Delta_{JT} = \frac{N\delta_{\Gamma}^2}{C_{\Gamma}^{(0)}}. \quad (26)$$

Hence, the concentration N of defect sites possessing electric quadrupole moments is obtained as follows:

$$N = \frac{\Delta_{JT} C_{\Gamma}^{(0)}}{\delta_{\Gamma}}. \quad (27)$$

From Eq. (16), the quadrupole-strain coupling constant g_{Γ} and the intersite quadrupole coupling constant g'_{Γ} have the following relationship with the effective charge Z^* and the effective radius of the quadrupole a^* :

$$\begin{aligned} g_{\Gamma} &= k_{\Gamma} Z^* a^{*2} \\ g'_{\Gamma} &= k'_{\Gamma} Z^{*2} a^{*4}. \end{aligned} \quad (28)$$

where k_{Γ} and k'_{Γ} are proportionality constants. From the above discussion, we obtain the following relationship between the deformation coupling energy δ_{Γ} , Z^* , and a^* :

$$\delta_{\Gamma} = \sqrt{\frac{2}{3}}g_{\Gamma} = \sqrt{\frac{2}{3}}k_{\Gamma} Z^* a^{*2} \quad (29)$$

5. COMPARISON OF SI AND DIAMOND

The energy gap between the valence and conduction bands for diamond is 5.45 eV, which is approximately five times larger than the 1.17 eV for Si with diamond structure as well. Thus, diamond is expected to be the ultimate semiconductor for outstanding high-power and high-frequency performance [1]. Other major properties are compared in the dyad and shown in Table AII.

TABLE AII. Comparison of various parameters between Si and diamond [24].

	Si	Diamond
Lattice constant: a	5.43 Å	3.567 Å
Nearest-neighbor distance: $\frac{\sqrt{3}a}{4}$	2.35 Å	1.55 Å
Melting point	1415 °C (1 atm)	~3550 °C (1 atm)
Density: ρ	2.33 g/cm ³	3.515 g/cm ³
Band gap	1.12 eV	5.45 eV
Cohesive energy (eV per atom)	4.63 ^a	7.37
Deformation binding energy: δ_{Γ}^0	2.28×10^9 K ^b	?
Magnitude of low-temperature softening (relative change in $\Delta C_{44}/C_{44}$)	1.6×10^{-4} (160 ppm) ^c	1.25×10^{-4} (125 ppm) ^d
Jahn-Teller energy: Δ_{JT}	0.51 mK	0.046 mK

^a See, M. Schlüter, Proc. Int. School of Physics “Enrico Fermi”, p.495 (1985), and references therein.

^b coupling constant of Boron-doped Si [34].

^c non-doped CZ-grown Si [37].

^d Type IIa HPHT diamond (present work).

6. MAGNETIC-FIELD DEPENDENCE OF THE SOFTENING OF C_{44}

The temperature dependence of the elastic constant C_{44} in the three types of diamonds, as shown in Fig. 3 of the main text, was studied as well in magnetic fields, as presented in Fig. A2. The results reveal that the HPHT type-Ib and type-IIa diamonds show small differences of C_{44} at 0 T and in a magnetic field of 16.5 T. However, CVD type-IIa diamond showed a slightly changed temperature dependence below 200 mK in a magnetic field of 14 T. This difference should be addressed in future investigations.

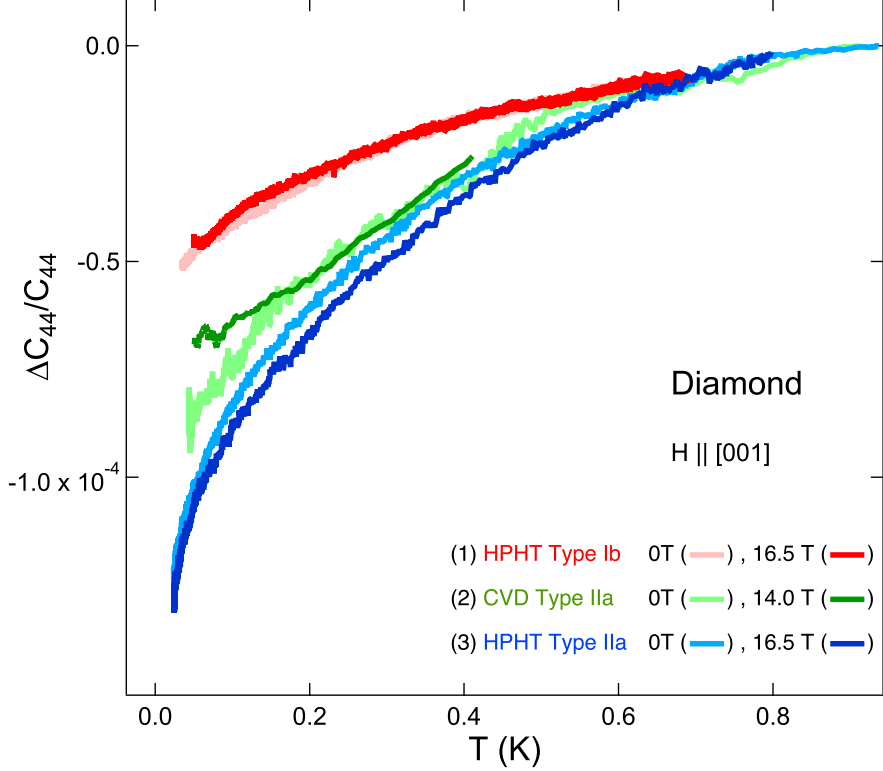


FIG. A2 Elastic softening of C_{44} for three different types of diamond at zero and magnetic fields of 16.5 or 14 T, applied for $H \parallel [001]$.

7. EFFECTS OF NV^- , NV_0 , AND NUCLEAR SPINS

In an NV center, the vacancy site exhibits reduced C_{3v} symmetry due to the substitution of one C atom by N, leading to a local symmetry breaking. Therefore, the sp^3 orbital splits into two a_1 singlets and one e doublet [49, 50]. When the nitrogen donor in the substituted position provides the carrier for the valence 1, the NV center is negatively charged (NV^-). According to Hund's first rule, the ground state adopts the highest value of total spin S , which is consistent with the Pauli exclusion principle. The six electrons occupy the a_1 singlets and the x and y orbitals of the e doublet to satisfy the condition that all wavefunctions are antisymmetric. Then, due to the spin-orbit interaction, the ground state of NV^- results in $S = 1$ or $S = 0$ ground state with irreducible representation 3A_2 , or 1A_1 . No electric quadrupole degrees of freedom exist in the 1A_1 singlet. Therefore, the e orbitals of NV^- do not contribute to the softening of C_{44} .

In this context, we also examine further possible scenarios. Stable isotopes of C include ${}^{12}\text{C}$, ${}^{13}\text{C}$, and ${}^{14}\text{C}$, with natural abundances of 98.9%, 1.1%, and $1.2 \times 10^{-8}\%$ and nuclear spin quantum numbers $I = 0, 1/2$, and 0, respectively. None of the isotopes has a nuclear quadrupole moment; hence, the elastic constants remain unaffected at zero magnetic field. The elastic constant depends hardly on magnetic fields and the change is negligibly small compared to the low-temperature softening. Thus, we conclude that the effect of ${}^{13}\text{C}$ is small and that nuclear spins need not to be considered.